Using Cryo-EM to Investigate Bacterial Secretion Systems

Chiara Rapisarda,[1,2,*] Matteo Tassinari,[3,4,*] Francesca Gubellini,[3,4] and Rémi Fronzes[1,2]

[1]Structure et Fonction des Nanomachines Bacte´riennes, Institut Europe´en de Chimie et Biologie, 33607 Pessac, France; email: c.rapisarda@iecb.u-bordeaux.fr, r.fronzes@iecb.u-bordeaux.fr

[2]CNRS UMR5234, Universite´ de Bordeaux, 33076 Bordeaux, France

[3]Institut Pasteur, Unite´ de Microbiologie Structurale, 75724 Paris, France; email: f.gubellini@pasteur.fr

[4]CNRS UMR3528, Institut Pasteur, 75015 Paris, France

Keywords

cryo-EM, cryo–electron microscopy, single particle, tomography, secretion systems, bacteria

Abstract

Bacterial secretion systems are responsible for releasing macromolecules to the extracellular milieu or directly into other cells. These membrane com- plexes are associated with pathogenicity and bacterial fitness. Understanding of these large assemblies has exponentially increased in the last few years thanks to electron microscopy. In fact, a revolution in this field has led to breakthroughs in characterizing the structures of secretion systems and other macromolecular machineries so as to obtain high-resolution images of com- plexes that could not be crystallized. In this review, we give a brief overview of structural advancements in the understanding of secretion systems, fo- cusing in particular on cryo–electron microscopy, whether tomography or single-particle analysis. We describe how such techniques have contributed to knowledge of the mechanism of macromolecule secretion in bacteria and the impact they will have in the future.

INTRODUCTION

Cryo-EM: Single-Particle Analysis and Tomography

The 2017 Nobel Prize in Chemistry was awarded to three pioneering scientists who developed cryo–electron microscopy (cryo-EM) for determining the high-resolution structure of biomolecules in solution: Jacques Dubochet, Joachim Frank, and Richard Henderson. This technique uses a beam of short-wavelength (high-energy) electrons to image biological assemblies that are invisible by conventional optical microscopes. The objects are either coated with heavy metal atoms (negative stain, NS) or flash frozen at low temperatures in liquid ethane to allow the formation of thin vitreous ice (31). NS-EM allows rapid screening and is convenient for macromolecules that either degrade when isolated or are dynamic complexes that form and break down quickly. Moreover, NS-improved contrast eases the characterization of new structural features. However, NS limits the resolution of the images and can cause artifacts in the sample. Frozen macromolecules better maintain their native conformation and can be imaged to obtain higher-resolution structures (50). Once the target macromolecules are imaged with an electron microscope, individual particles are aligned and attributed an orientation, and a 3D reconstruction of the object is calculated (38). In single-particle analysis (SPA), several thousands of randomly oriented particles are imaged, selected, and analyzed. Electron cryotomography (ECT) can also be used to obtain 3D structures of large macromolecular complexes and entire cells. This approach captures images of individual assemblies from multiple angles to obtain information in 3D (111).

EM changed the way we investigate biomolecular assemblies. Precise knowledge of the structure of macromolecular assemblies is crucial for understanding their function. Until 2014 the structure of proteins at a resolution below 4 Å was only obtained through the use of X-ray crystallography. Since then, cryo-EM has been steadily producing structures at near-atomic resolution. This has been called the cryo-EM resolution revolution and was due to several concomitant technological advances (63). First and foremost, direct detector cameras provided rapid electronic readout and movie recording at up to 40 frames per second (67). This allows for the correction of sample drift that occurs during imaging. Moreover, the advent of automated data acquisition allowed collection of thousands of images of particles, required for obtaining high-resolution

Cryo–electron microscopy (cryo-EM): electrons passing through a sample frozen in very thin vitreous ice are absorbed by the atoms in the sample, creating a 2D image

Resolution: the shortest distance that can be discerned between two objects; at a resolution of 4 Å, only objects ≤ 4 Å apart can be correctly identified

Negative-stain EM (NS-EM): a large molecular weight stain impermeable to the electrons passed through the sample creates a negative image in which the object is lighter than the background

Dynamic complexes: protein complexes that assemble, disassemble, or change shape

structures (49). Finally, new open-source image-processing software (101, 106) has made it rel- atively easy to analyze images of complex samples due to their heterogeneity (i.e., including a particular ligand/component in only part of the population) and flexibility (i.e., proteins present- ing different conformations in the same sample). These samples were previously unsuitable for structural analyses requiring ordered arrays of molecules.

Secretion Systems and Cryo-EM: A Historical Perspective

Bacteria need to communicate with, antagonize, or collaborate with other cells, whether prokary- otic or eukaryotic. To do so, they secrete numerous macromolecules, also called effectors, in the extracellular milieu or directly into the other cells. To be secreted, effectors have to cross one or two largely impermeable lipid bilayers that enclose the bacteria, and such a process requires energy. This is particularly difficult in didermal (gram-negative and mycolic acid–containing) bacteria. Membrane-spanning secretion systems evolved as specialized macromolecular nanomachines that provide energy and a channel for secreting a variety of substrates (113). Released macromolecules include DNA, polysaccharides, proteins, enzymes, and toxins targeting other prokaryotes or eu- karyotes. Nine secretion systems have been identified: types I through IX, numbered in the order in which they were discovered (1) (**Figure 1**). They are usually encoded as operons in the genome or in plasmids. Each bacterial species can express none, one, or more types of secretion systems; often their presence in the genome is correlated with pathogenicity (37, 86, 114). Secretion can occur through a one-step mechanism (**Figure 1*a***) where the effector is transported through a channel from the cytoplasm to the extracellular milieu (types I, III, IV, VI, and VII). In other cases the macromolecules are secreted during a two-step mechanism: First they are transported through the Sec/Tat systems to the periplasm, and from there they are released in the extracellular space through one of the two-step secretion systems (types II, V, VIII, and IX) (**Figure 1*b***).

Most secretion systems, especially the one-step secretion systems, are unsuitable for X-ray crystallography because they are dynamic machines composed of several dozens of different, highly oligomeric proteins and spanning one or both bacterial membranes. Attempts at crystallizing large membrane complexes have proven futile in most cases. Notable exceptions are the type I (77) and type IV (40) secretion systems (T1SS and T4SS). Most often, a divide-and-conquer approach was commonly used to obtain structures by X-ray crystallography of isolated components of each assembly. However, the structural information revealing the global architecture of a complex is necessary to understand its function and its mechanism of action. With an arsenal of X-ray and/or NMR structures previously available and the recent advancements made during the cryo-EM resolution revolution, the last few years have seen a drastic increase in the number of structures deposited in the Electron Microscopy Data Bank (EMDB) of assembled secretion systems obtained by NS- and cryo-EM, by both SPA and ECT.

In this review, we highlight some of the most compelling advances in the knowledge of bacterial secretion systems. We cover only the secretion systems for which NS- and cryo-EM have been used extensively, namely, types II, III, IV, VI, and VII. Other secretion system structures have been investigated mainly by X-ray crystallography (types I, V, VIII, and IX). We refer readers to other reviews to learn about these secretion systems not discussed here and their effectors' mechanisms of action (36, 46, 65, 77, 93).

Single-particle analysis (SPA): isolated proteins embedded in NS or frozen in vitreous ice, ideally in different orientations, are imaged in an electron microscope to construct a 3D model

Electron cryotomography (ECT): an object frozen in vitreous ice is imaged at different angles to reconstruct its 3D image

X-ray crystallography: X-rays scatter from a crystalline object to obtain their 3D form

Effectors: macromolecules secreted by the secretion systems that may have different effects on the target cell

Secretion: active transport of macromolecules (proteins or DNA) across one or two lipid membranes

Electron Microscopy Data Bank (EMDB): official repository of electron density maps obtained by ECT and SPA

THE TYPE II SECRETION SYSTEM AND THE RESOLUTION REVOLUTION

The T2SS was one of the first bacterial secretion systems to be identified. In the 1980s it was reported to promote secretion of a folded enzyme, pullulanase, in *Klebsiella oxytoca* (29).

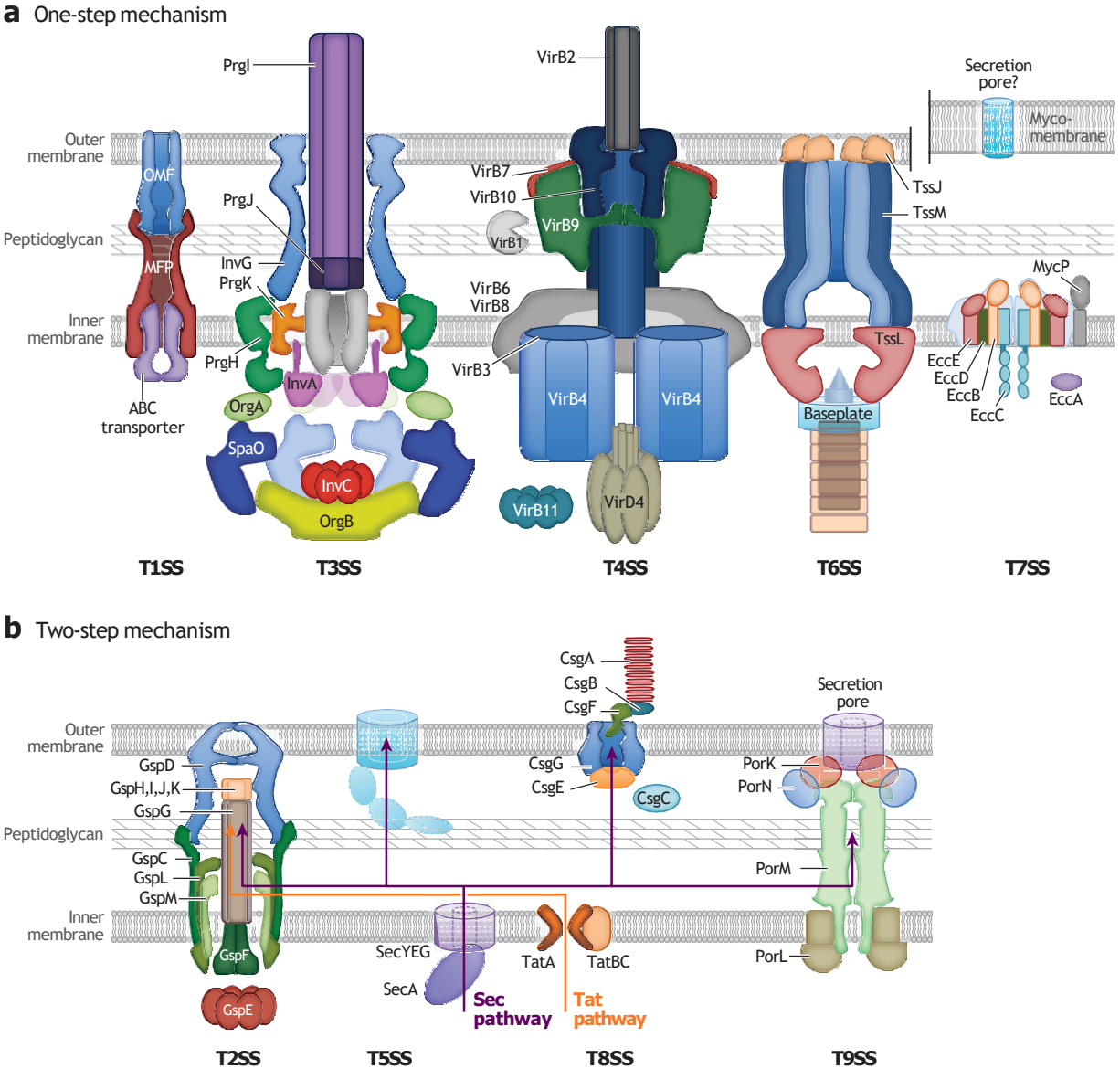

Figure 1

Schematic of secretion systems in didermal bacteria. (*a*) Five kinds of secretion systems use mainly a one-step secretion mechanism: type I secretion systems (T1SSs), T3SSs, T4SSs (T4ASS shown), T6SSs, and T7SSs (ESX-5 shown). The mycomembrane is indicated separately for the T7SS. (*b*) Secretion systems using mainly a two-step secretion mechanism are T2SSs, T5SSs, T8SSs, and T9SSs. The general secretion pathway (Sec pathway) and the twin arginine translocation (Tat) pathway, which perform the first secretion step into the periplasmic space, are also indicated.

Subsequently discovered in many other gram-negative bacteria, this system was designated one of the terminal branches of the general secretion pathway (Gsp) (89). The T2SS shares homology with the type IV pilus assembly apparatus and is found exclusively in gram-negative bacteria (51). It is involved in the secretion of numerous effectors that are required not only for pathogenicity but also for the establishment of symbiotic relationships. Along with the T6SS (104) and T9SS (65), the T2SS is able to secrete proteins in their folded states. The T2SS belongs to the subgroup of two-step secretion systems, together with the T5SS (36), T8SS (46), and T9SS (65). Secretion in these systems does not occur through a single continuous channel between the inner and outer membranes; rather, it requires two distinct machineries. Some newly synthesized effectors, such as *Klebsiella* pullulanase, are exported as unfolded polypeptides to the periplasm through the Sec pathway and fold in the periplasm (90); others, such as phospholipase C in *Pseudomonas aeruginosa*, need to be translocated in a folded state through the Tat protein export system (110) (**Figure 1*b***). Once in the periplasm, they are secreted as fully folded proteins or in some cases as protein complexes (e.g., cholera toxin from *Vibrio* species) through the T2SS outer membrane channel named secretin. The signal for secretion is still unknown, and it is species specific (68); however, structural elements such as loop-containing subdomains rich in polar residues have been implicated in secretion of pullulanase (35) and of PelI effector of the *Dickeya dadantii* T2SS (87).

T2SS genes are organized in most proteobacteria in an operon encoding 12–15 proteins, 11 of which are essential to secretion (GspC-M, **Figure 2*a***) (89). These proteins assemble into two main subcomplexes (**Figure 2*b***): an inner membrane complex required for the polymerization of a pseudopilus, similar to the type IV pilus (T4P) (85), and an outer membrane secretin that shares a common ancestor with the channels of T3SS (58), T4P (27), and protein IV (pIV) from the filamentous phage (69). A cytoplasmic secretion ATPase (GspE) provides the energy for pilus assembly by the inner membrane complex (100). The pseudopilus (GspG and minor pilins GspH, I, J) probably acts as a piston or as a screw (81) to push the folded effector or toxin through a large pore composed of multiple subunits of the secretin protein (GspD; **Figure 2*b***) (84). The secretin is one of the best examples of recent progress in cryo-EM (**Table 1**, **Figure 2*c***). Improvement in the resolution of the secretin structure contributed to a better understanding of the architecture and function of the whole complex. In 1997 the first scanning electron micrograph of the closely related pIV revealed the formation of a cylindrical structure composed of 14 copies of the secretin subunit (69). In 2005 the first SPA cryo-EM structure of the T2SS secretin in *K. oxytoca* at 22 Å resolution confirmed the dodecameric nature of the assembly and the presence of a plug (also present in the T3SS and the T4P) in the saucer-like structure forming a barrier that prevents leakage of the periplasm out of the cells (**Figure 2*c***). The structure of the secretin also allowed the identification of two distinct domains, the C- and N-terminal domains (20). The improved structure at 19 Å in 2010 of the *Vibrio cholerae* secretin was also dodecameric and allowed for the fitting of X-ray structures of the different N-terminal domains and the identification of an extracellular plug in addition to the periplasmic plug, identified as the N3 domain (**Figure 2*c***). The authors who reported this proposed that the periplasmic plug, not conserved among species, determines the selectivity filter for the substrate and that the gate would be opened up by the pilus assembly acting as a piston (95).

More recently, several new structures reached subnanometer resolutions and allowed for a finer understanding of the elusive mechanism of secretion. The first structure at 8.2 Å made it possible to identify several notable features that were missed previously, such as the presence of a periplasmic grid that allows the passage of solutes through the channel (**Figure 2*d***). A cavity was also present at the level of the outer membrane domain that resembled those found in pore-forming toxins (**Figure 2*d***). Because of this structural similarity, it was proposed that the C-terminal domains of the secretins undergo a conformational change upon contact with the membrane to allow for

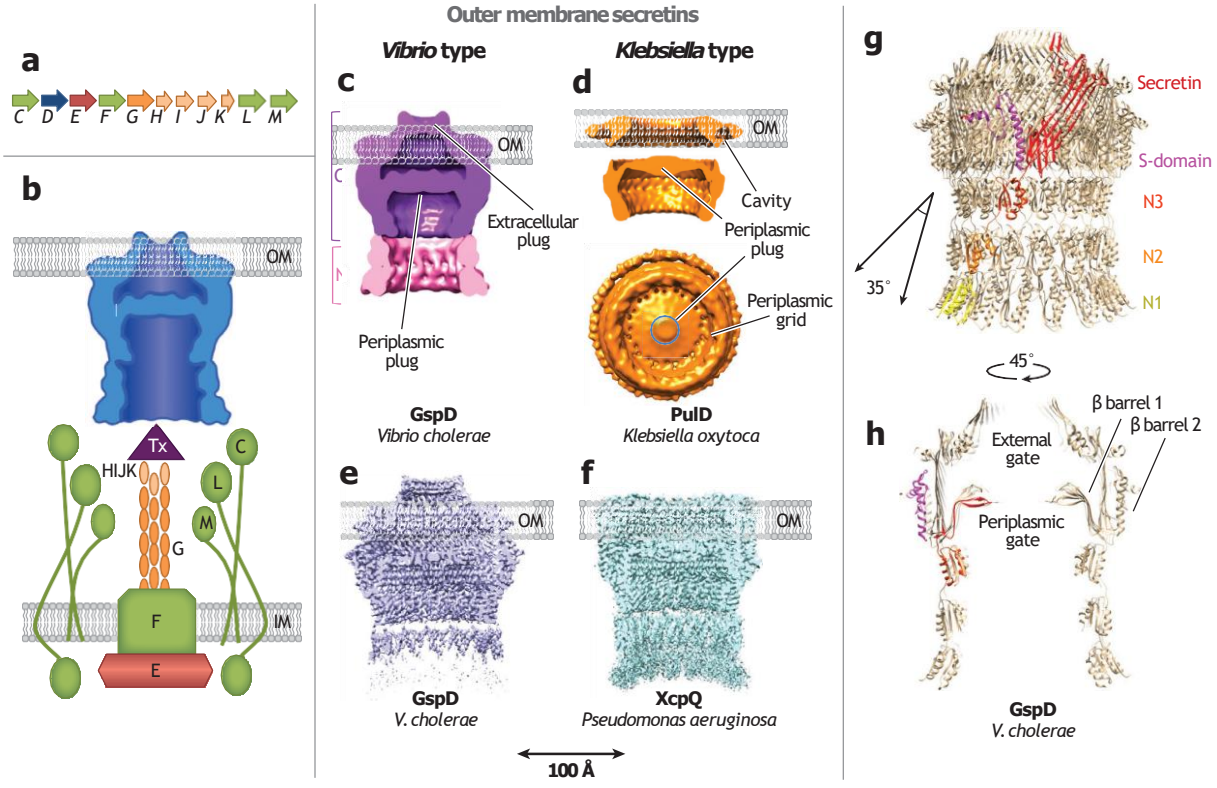

Figure 2

(*a*) The typical gene organization of the general secretion pathway (Gsp) of the type II secretion system (T2SS). In green are the proteins that constitute the inner membrane (IM) complex. In blue is the outer membrane (OM) secretin and in red is the ATPase that powers secretion. The pilus is composed of the major pilus (G) and the minor pilins (HIJK). (*b*) The T2SS is mainly composed of an inner membrane complex (*green*) and a secretin (*blue*) that forms a pore in the outer membrane. The translocation of the toxin/effector (Tx, *purple*) mediated by pilus assembly is powered by the ATPase E. (*c–f*) Type II outer membrane secretins can be divided into two subclasses, the *Vibrio* type and the *Klebsiella* type, based on their sequence and structure. (*c*) Cross-section of the cryo-EM structure of the secretin *Vibrio cholerae* GspD structure at 19 Å (EMD-1763). The periplasmid and the extracellular gates are indicated. The N-terminal domain is in pink and the C-terminal domain in purple. (*d*) Cross-section of PulD from *Klebsiella oxytoca* at 8.2 Å resolution (EMD-2628). Labels show the cavity that inserts in the membrane, the periplasmic plug, and the periplasmic grid that allows solutes to pass. (*e*) Cross-section of GspD from *V. cholerae* at 3.26 Å (EMD-6676). (*f*) Cross-section of XcpQ from *Pseudomonas aeruginosa* at 3.57 Å (EMD-6675). (*g*) Atomic model of the GspD protein from *V. cholerae*, built from the cryo-EM density EMD-6676, with different domains. (*h*) Cross-section of the atomic model of GspD from *V. cholerae* rotated 45°. The external gate and the periplasmic gate are visible, as well as the two concentric β barrels in the secretin domain.

their insertion and pore formation. In the periplasmic portion of the complex, the electron density showed that the cup was composed of two distinct protein layers that overlap each other, thus protecting them from trypsin cleavage (107). Only when the resolution increased to better than 4 Å were researchers able to obtain the full atomic details by cryo-EM of the secretin protein in *V. cholerae* (117) (**Figure 2*e***), *Escherichia coli* K12 (117), *P. aeruginosa* (48) (**Figure 2*f***), and enteropathogenic *E. coli* (EPEC) (47). At such resolution, the crystal structures of the 3 N domains (N1, N2, N3) and the C-terminal domains (secretin and S-domain) were accurately placed in the electron density and regions whose structures were previously unknown, where built de novo (**Figure 2*g***).

Table 1 Secretins of type II secretion cryo-EM structures

Secretin	Species	Resolution (Å)	EMDB No.	Oligomerization	Ref.	Year
PulD	*Klebsiella oxytoca*	NA	NA	12	84	1999
PulD	*Klebsiella oxytoca*	22	NA	12	20	2005
GspD	*Vibrio cholerae*	19	1763	12	95	2010
PulD	*Klebsiella oxytoca*	8.2	2628	12	107	2014
GspD	*Vibrio cholerae*	3.26	6676	15	117	2017
GspD	*Escherichia coli* K12	3.04	6675	15–16	117	2017
XcpQ	*Pseudomonas aeruginosa*	3.57	8860	15	48	2017
GspD	EPEC	4.2	8779	15	47	2018

Abbreviations: EMDB, Electron Microscopy Data Bank; EPEC, enteropathogenic *Escherichia coli*; NA, not available.

The atomic model of the secretin, thus constructed, is well conserved across species and in the T3SS, with the exception of the extracellular plug that is present only in the *Vibrio*- type T2SS (**Figure 2*c*,*e***). The overall shape of the C terminus consists of an S-domain required for the contact between two monomers and the secretin domain, composed of two layers of the barrel, previously observed in the lower-resolution structure, and now identified as two concentric β barrels (**Figure 2*h***), one of which forms the periplasmic gate (**Figure 2*g*,*h***). The periplasmic grid was found to be an artifact in the data analysis, since in the high-resolution structures no pores were found at the level of the periplasmic plug. Each monomer of the secretin extends from the C-terminal β barrels, which are inserted in the membrane, toward the periplasm at ∼35° compared to the barrel axis in all the structures (**Figure 2*g***). Some inconsistencies were observed in the symmetry of the molecules since the *Vibrio* structures appear to have 12-fold or 15-fold symmetry in the low- or high-resolution structures, respectively (95, 117). Such disparity could be attributable to the sample preparation or to the dynamic assembly of the secretin monomers, also observed in the varying symmetry of the *E. coli* K12 structure (117). Finally, of note, these structures have confirmed the previous subclassification of T2SS secretins based on primary sequence (32) into two distinct types (**Table 1**, **Figure 1**): the *Vibrio* type and the *Klebsiella* type (47) (**Figure 2*c*–*f***). The overall structure is well conserved between the two, but *Vibrio*-type members, including *V. cholerae* and EPEC, have an additional cap or extracellular gate that extends beyond the outer membrane and could be crucial to secretion (**Figure 2**). Moreover, the cap appears to be too narrow to allow the folded substrate to pass, indicating that the type II secretin might undergo a conformational change during secretion (**Figure 2*c*–*f***).

Although no structure of the full T2SS complex is yet available, the closely related T4P assembly machine was uncovered by ECT and the locations of all its components mapped on the complex by systematic deletions. This structure, as well as the structure-function analysis of the pseudopilus assembly in the *Klebsiella* T2SS model (81), is consistent with the mechanism of pilus assembly led by rotation of the only component in the inner membrane assembly that is free to rotate, GspF (**Figure 2*b***). Such rotation would allow the addition of pilin subunits at the base of the fiber with minimal energy and power the pilus elongation (23, 81). So far, in the T2SS, the only high- resolution structure available for the pseudopilus outer membrane subcomplex has been obtained by cryo-EM (70). Yet, detailed structural information obtained by other techniques is available for nearly all soluble domains of the T2SS components (82). These data combined with SPA and ECT should be invaluable to uncover the structure of the T2SS as a whole complex and gain insights into the pseudopilus assembly and the secretion mechanism. Further work would need to be carried out to understand how the pseudopilus and the other components are assembled

Atomic model: a structure revealing the position of atoms in an amino acid chain; at <3 Å each atom's position is visible

Symmetry: the number of times a protein unit is repeated in a complex; referred to here as an X-fold symmetry, with X indicating the smallest repeating unit

and how they function. Such work will require the structural characterization of the full complex spanning the two membranes by ECT, as was done for the T4P (23). Moreover, due to their sequence diversity, the structures of secretins from species such as *Legionella* spp. and *Acinetobacter* spp. will allow us to better classify these assemblies and to better understand the mechanism of effector secretion selectivity (30).

THE TYPE III SECRETION SYSTEM: THE BACTERIAL INJECTISOME

The T3SS is a sophisticated macromolecular machine found in a number of gram-negative bacteria whose role is to inject effector proteins directly into the cytosolic compartment of infected host cells. A large variety of human and plant pathogens, such as *Yersinia* spp., *Salmonella* spp., *Shigella* spp., *Bordetella* spp., *P. aeruginosa*, and EPEC, encode one or several T3SSs (54). They release several types of effectors that manipulate the host cell by a range of mechanisms, such as disrupting phagocytosis, rearranging the cytoskeleton, or inducing apoptosis (93). The T3SS is made up of more than 20 proteins and is broadly conserved across species, in a one-step mechanism (**Figure 1*a***) for secreting a diversity of substrates. It is composed of a basal body forming a continuous channel across the inner and outer membranes, a needle, an ATPase-containing sorting platform, and an export apparatus (43, 83) (**Figure 3*b***). In the last two decades the T3SS has been studied in different species and conditions, and robust cryo-EM data, both SPA and ECT, have been obtained to determine the precise position of most subunits (**Figure 3**).

The first cryo-EM structure at 17 Å resolution of the *Salmonella* T3SS complex was published in 2004 (76); with the EM resolution revolution, it improved to 11.7 Å and finally 4.3 Å (**Figure 3*a***). The resolution of the first structure was too low to allocate the single subunit position to the density map or to infer the symmetry; nevertheless, this pioneering work ushered in a new era of cryo-EM characterization of bacterial membrane macromolecular complexes. The basal body, composed of several rings of proteins (InvG, PrgH, and PrgK), shows a characteristic nut-and-bolt architecture (**Figure 3*b***). InvG is a member of the family of pore-forming secretins (also found in the T2SS and T4P), and it is the only protein of the apparatus located in the outer membrane (73, 107). An InvG homolog from *Yersinia pestis*, YscC, was previously observed by NS-EM to assemble in a 1-MDa structure (16). Being long enough to span the periplasmic space, it projects to the extracellular space an ~50-nm-long needle filament composed of multiple copies of the protein PrgI (**Figure 3*b***).

At the level of the inner ring, a cup-like protrusion extending to the cytoplasm is the entry point to the secretion channel. The periplasmic components of the T3SS define a hollow chamber with a socket structure at the base, probably functioning as a docking platform for the inner rod assembly made by PrgJ (76) (**Figure 3*b***). The socket is connected with the inner rod, which becomes the needle filament (PrgI) corresponding to the outer ring (**Figure 3*b***). *Salmonella enterica* Typhimurium strains lacking the InvJ ruler protein are known to assemble a T3SS equipped with a very long and easily detachable needle filament (114). The structure of the T3SS from a ΔInvJ strain solved at 20 Å resolution (75) completely lacks the socket apparatus and has a smaller cuplike protuberance. In the absence of the inner rod and needle filament, the outer ring adopts a closed conformation (75). This has led to the hypothesis that the needle filament components and the first set of substrates secreted, PrgJ and PrgI, start polymerizing the inner rod and the needle filament. Once PrgJ subunits grow throughout the periplasmic chamber, InvJ induces a conformational change that arrests needle growth and the T3SS switches to the secretion of a second set of substrates, the effector proteins (56).

Schraidt & Marlovitz (103) were the first to obtain a cryo-EM structure of the T3SS at subnanometer resolution (**Figure 3*b***). The electron-density map offered the possibility to distinguish and allocate the single components, InvG, PrgH, and PrgK, over a 3.5-MDa structure,

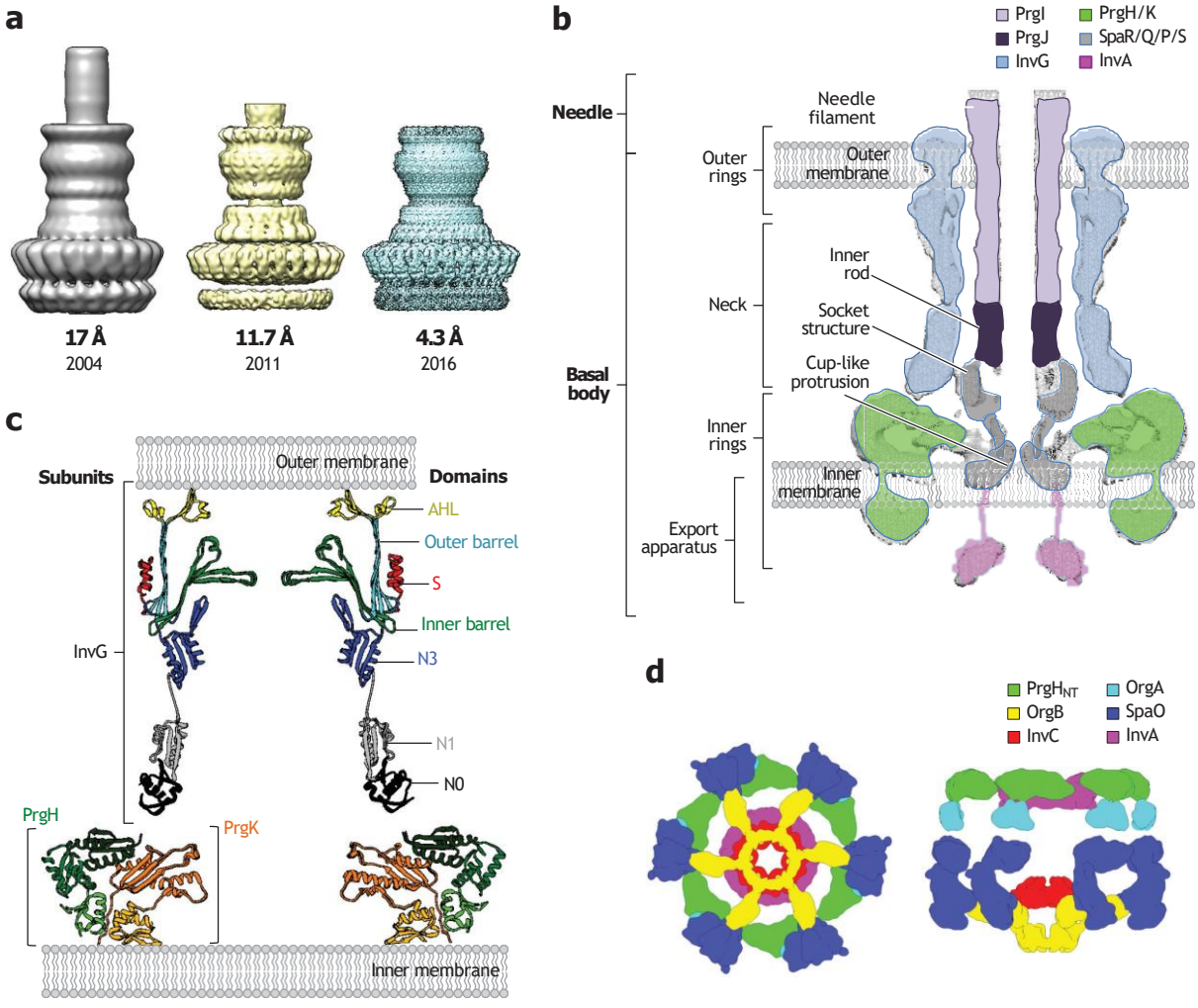

Figure 3

Structural architecture of the type III secretion system (T3SS). (*a*) Scheme showing the improvement in resolution for the T3SS over time: (*left to right*) needle complex at 17 Å obtained in 2004 (Electron Microscopy Data Bank number EMD-1100), an 11.7-Å reconstruction obtained in 2011 (EMD-1875), and a 4.3-Å resolution structure, currently the highest resolution achieved for the T3SS basal body (EMD-8398). (*b*) Scheme of the needle complex drawn on a section of the model EMD-1875. The external and internal modules are indicated by brackets and lines, respectively. (*c*) Atomic model of the T3SS periplasmic region, including domains of the secretin and the subunits PrgK and PrgH forming the basal body rings (from EMD-8389). The subunit names are indicated on the left side, while the domains composing the secretin, InvG, are labeled on the right side. (*d*) The T3SS sorting platform structure obtained via electron cryotomography (EMD-2667), as viewed (*left*) from the bottom and (*right*) from the side. The subunits are distinguished by different colors.

in accordance with previous topology assignments (102) and crystal structures (105, 118). The inner rings are assembled as 24 monomers of PrgH and PrgK, arranged concentrically; the soluble domains of PrgH form the external ring and those of PrgK the internal one (**Figure 3*c***). The densities for their transmembrane, C-terminal, and N-terminal regions, which were missing in the crystallographic structure, were present but were not well resolved in the cryo-EM density map. Docking of the crystal structures in this map allowed an atomic model of the basal body to

be built. The cryo-EM structure of the injectisome with a substrate trapped inside showed that no substantial conformational change takes place in the secretion pores (92).

Subsequently, the structure of a secretion-deficient mutant *S.* Typhimurium basal body, as- sembled with an N-terminal $PrgH^{130–392}$ deletion, was determined at 4.3 Å, imposing a 24-fold symmetry, which made it possible to build an atomic model de novo for most of the inner mem- brane rings, comprising $PrgH_{171–364}$ and $PrgK_{20–203}$ (116) (**Figure 2*c***). In this work the outer InvG secretin pore was purified separately, and its structure was refined to 3.6 Å with a 15-fold sym- metry (116) (**Figure 3*c***). Most of the secretin sequence, except domains D0 and D1, is built in the atomic model. Just as in the GspD type II secretin (**Figure 2**), the walls of the main body are made of eight-stranded β sandwiches assembled in an outer barrel, with a second, inner barrel forming a gate responsible for the closed conformation of the secretin complex. In the upper part of the structure, a single amphipathic helical loop (AHL) is inserted in the outer membrane. At the C terminus, the S-domain is folded beside the external barrel. It carries a helix-turn-helix motif recognized by the chaperone pilotin, which mediates the outer membrane insertion (57). Downstream, three N domains contain the ring-building motif (RBM) (105). While N3 is still part of the outer core, stabilizing the gate, the neck of the T3SS basal body comprises domains N0 and N1(**Figure 3*c***).

The T3SS complex also possesses a large cytoplasmic apparatus involved in substrate entry into the needle complex. This region is very dynamic and unstable and has been mostly studied by ECT, since this technique allows direct observation of the secretion machinery in situ. The T3SS from *S.* Typhimurium (52), *Shigella flexneri* (53, 74), *Chlamydia trachomatis* (78), and *Yersinia enterocolitica* (61) have been studied by ECT. The best characterized apparatus is the injectisome in
S. Typhimurium, whose structure was determined to 17 Å by subtomogram averaging, displays the typical segments identified by SPA cryo-EM (inner rings, neck, and outer rings), with the local inner membrane clearly visible, corresponding to the T3SS insertion. Underneath the socket structure the subtomogram averaging shows density for the export apparatus, formed by four membrane proteins, SpaR, SpaQ, SpaP, and SpaS. The composition of this cuplike structure (**Figure 3*b***), with the aperture partially occupied by the socket and the base spanning the inner membrane, was further confirmed by SPA cryo-EM of its components (64). The subunits SpaP, SpaQ, and SpaR form a right-handed helical assembly that fits well in the cup and socket densities of the *Salmonella* needle reconstruction (103).

Looking at the cytoplasm, a toroidal shape is organized by InvA and together with the cuplike structure composes the export apparatus. Systematic deletion of T3SS genes, in combination with the use of traceable proteins, facilitated the localization of each component in the tomograms. The sorting platform consists of six pods made by OrgA and SpaO and linked together through OrgB at the center by the hexameric ATPase InvC (**Figure 3*d***). The center of the sorting platform resembles a wheel-like structure facing the cytoplasmic domain of the nonameric InvA. As in the injectisome basal body, from the OrgA pods to the PrgH there is a symmetry transition, in this case from a 6-fold to a 24-fold symmetry.

In conclusion, ECT offered an unprecedented view of the *Salmonella* T3SS, highlighting ar- chitectures difficult to detect by SPA: the export apparatus and the sorting platform. The overall architecture of the needle complex resembles closely that obtained by SPA cryo-EM. Moreover, the sorting platform builds a cage-like structure contacting the N-terminal domain of PrgH. The power unit of the system is represented by the hexameric ATPase InvC, localized in the center of the sorting platform, which drives the overall 6-fold symmetry; it furnishes the energy for the substrate unfolding and translocation into the secretion channel.

Despite the high resolution obtained for the T3SS needle complex, there are still open ques- tions. In particular, the conformational changes required for substrate secretion, the mechanism

Translocation: active transport of macromolecules across a membrane

that triggers gate opening, and the reorientation of the secretin N3 domain are still unknown. A high-resolution structure of the needle complex occupied by the substrate could unveil key subdomains involved in the effector translocation. Furthermore, the molecular basis for the T3SS conformational switch between an InvI-InvJ and effector protein secretion modes needs to be determined. It is unclear whether the architecture observed by ECT is necessary for both T3SS states, considering the available data on the whole mechanism for substrate recruitment; further work is needed to answer all these questions.

TYPE IV SECRETION SYSTEMS: VERSATILE NANOMACHINES

T4SSs are versatile machineries that help increase bacterial fitness and survival in different ways. Their broad phylogenetic distribution includes gram-negative and gram-positive bacteria as well as some archaea. Phylogenetic analysis and available structural information divide this family into two subgroups: T4ASS and T4BSS (3, 25).

Type IVA Secretion Systems

The T4ASS mediates the conjugative transfer of genetic material between two cells. DNA exchange favors genome plasticity and is a major cause of antibiotic resistance. However, some intracellular human pathogens (such as *Brucella* spp., *Bartonella* spp., and *Rickettsia* spp.) use the T4ASS to secrete effector proteins into their host. The VirB/D4 system encoded by the Ti plasmid of the plant pathogen *Agrobacterium tumefaciens* is the paradigm for conjugative secretion systems. It transfers the T-DNA and its associated proteins into the host cell, inducing plant tumors and providing a favorable environment for the bacterium to grow (44). Closely related T4ASSs are expressed by the *E. coli* conjugative plasmids [such as the F-plasmid, pKM101, RP4, and R388 (8)] transferring genetic materials between two cells through the pilus (66).

Crucial biochemical and functional data have been obtained through extensive investigation of T4SSs (19, 25, 41). However, understanding of their mechanism was impeded by the absence of structural evidence of assembled systems. Such structures were recently obtained using EM and X-ray crystallography of systems encoded by conjugative plasmids R388 and pKM101. These are composed of 12 subunits (here named VirB1 to VirB11, as in *A. tumefaciens*, and VirD4) (**Figure 4*a***).

The first structure revealing insights in the overall organization of a T4ASS was the one from the pKM101 core complex (CC) obtained by cryo-EM (40) (**Figure 4*b***). This CC is an ~1.1-MDa complex formed by 14 copies each of subunits VirB7, VirB9, and VirB10 (**Figure 4*b***). Its 3D structure was obtained by cryo-EM, first at 15 Å (42) and then at 12.4 Å (96) (**Figure 4*b***). The CC measures 185 Å in height and diameter. It is composed of an outer layer (O-layer) inserted in the outer membrane and a subjacent inner layer (I-layer). The crystal structure of the O-layer revealed the CC subunits' positions (**Figure 4*b***). VirB7, anchored to the outer membrane, defines most of the external wall of the O-layer. It interacts only with VirB9, which in turn interacts with VirB10. VirB10 builds the inner wall of the O-layer and has an important role in stabilizing the whole structure (10, 21, 42). The I-layer defines an inner chamber surrounded by two walls, clearly defined in the cryo-EM structure at 12.4 Å. At the CC base, a pore of 55-Å diameter is observed. The inner chamber is separated from the overlying outer chamber by the middle platform, a flexible structure probably formed by both VirB9 and VirB10. On top of the CC, a pore, 20 Å in diameter, opens to the extracellular space.

A truncated version of this CC yielded a cryo-EM structure at higher resolution (8.5 Å) (96) revealing that the N-terminal region of VirB10 forms the inner wall of the I-layer. This structure

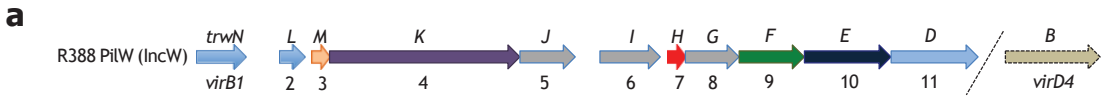
a
R388 PilW (IncW)
trwN
virB1
L M K J I H G F E D B
virD4
2 3 4 5 6 7 8 9 10 11

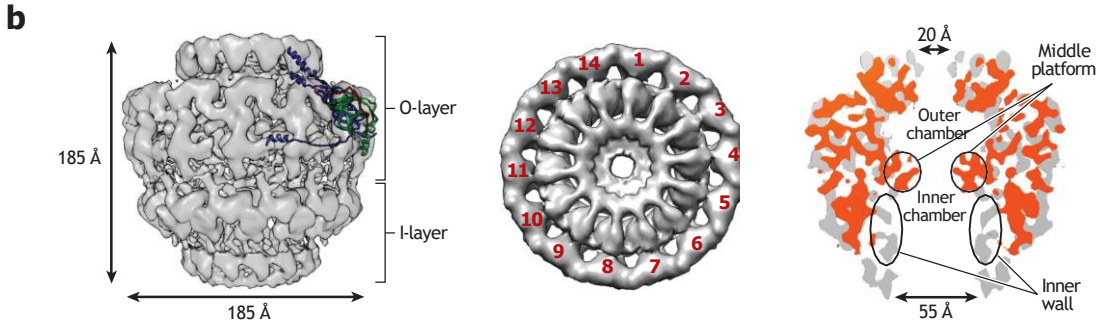
b
185 Å
O-layer
I-layer
185 Å
14 1 2 3 4 5 6 7 8 9 10 11 12 13
20 Å
Middle platform
Outer chamber
Inner chamber
Inner wall
55 Å

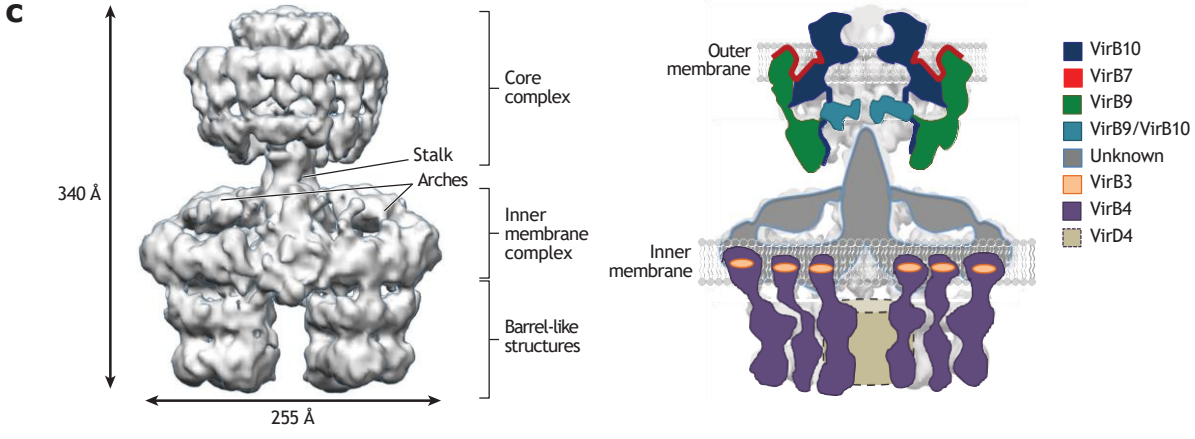
c
340 Å
Core complex
Stalk
Arches
Inner membrane complex
Barrel-like structures
255 Å
Outer membrane
Inner membrane
VirB10
VirB7
VirB9
VirB9/VirB10
Unknown
VirB3
VirB4
VirD4

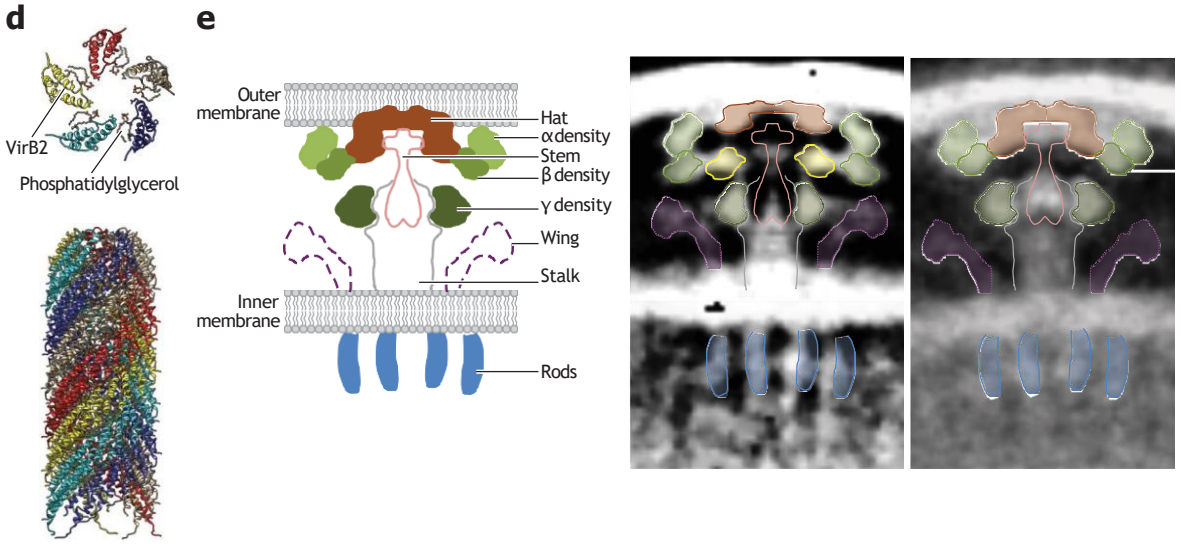
d
VirB2
Phosphatidylglycerol
e
Outer membrane
Hat
α density
Stem
β density
γ density
Wing
Stalk
Inner membrane
Rods

Figure 4 (*Figure appears on preceding page*)

Structures of the type IV secretion systems (T4SSs) obtained by single-particle analysis and electron cryotomography. (*a*) Genetic organization of the T4SS cluster from the *Escherichia coli* R388 plasmid. (*b*) Structures of the T4ASS core complex (CC) from the pKM101 conjugative plasmid. (*Left*) CC_{FL} (Electron Microscopy Data Bank number EMD-2232) superimposed on the heterotrimeric crystallographic unit. (*Center*) The CC_{FL} top view shows a 14-fold symmetry organization. (*Right*) Section of the side view of the CC_{FL} (*grey*) and the $CC_{ELASTASE}$ (EMD-2233, *orange*), superimposed. The main differences between the two structures are outlined by circles. The different conformation of the middle platform is visible, dividing the inner and upper chambers. The inner wall is absent in the $CC_{ELASTASE}$ structure. (*c*) 3D model of $T4SS_{3-10}$ (EMD-2567) from the conjugative plasmid R388. (*Left*) Side view. The CC, stalk, and inner membrane complex (IMC) are indicated. The two barrel-like structures in the IMC are composed of VirB4 hexamers. (*Right*) Schematic representation of the $T4SS_{3-10}$. Different colors indicate the various components of the structure. (*d*) Atomic model of the F-like pilus encoded by the pED208 plasmid (EMD-4042). The pilus assembly (*top*) is given by VirB2 pentamers stacked on top of each other (*bottom*). VirB2 monomers are present in a 1:1 ratio with phosphatidylglycerol. (*e*) In situ T4SS. (*Left*) schematic representation of the T4SS showing the different components, as in the Dot/Icm complex (45). (*Center*) Subtomogram averages of *Helicobacter pylori* cag T4SS obtained by electron cryotomography. The subtomograms EMD-7474 and EMD-7475 have been overlapped and colored as in the scheme. An additional δ density is highlighted in yellow. (*Right*) Subtomogram averages of *Legionella pneumophila* Dot/Icm obtained by electron cryotomography. The subtomograms EMD-8566 and EMD-8567 have been overlapped and colored as in the scheme on the left.

suggests that VirB10 plays a role in the conformational change of the middle platform (**Figure 4*b***) during substrate translocation.

The structure of a partially assembled T4ASS from the R388 plasmid was solved by NS-EM (~20 Å) (72). This $T4SS_{3-10}$ complex (~3 MDa) included subunits VirB3 to VirB10. It showed a large inner membrane complex (IMC) subjacent to the characteristic structure of the CC. The IMC presents two membrane-associated arches, and it is linked to the CC through a stalk, formed by the N-terminal region of VirB10 and maybe other subunits. Limited contacts between the stalk and the CC resulted in high flexibility of the complex at this level. Together, the stalk and the CC span the periplasm up to the bacterial outer membrane (**Figure 4*c***).

The cytoplasmic ATPase VirB4 is located at the base of the IMC, forming a barrel-like structure. Recently it was shown by NS-EM that the ATPase VirD4, the coupling factor essential for substrate recognition (17), associates with the assembly in between these barrels (94). The location of the third ATPase (VirB11) on the system is still unknown.

The subunit VirB3 is associated with VirB4 in the membrane portion of the IMC. The exact position of other subunits, i.e., the multiple-membrane-spanning proteins VirB6, VirB5, and VirB8, has not been determined yet.

Extending from the top of the CC, the pilus connects the donor and the recipient cells during conjugation, transferring the DNA-relaxase complex in an unfolded state (108). The structure of the DNA-relaxase complex was recently solved by cryo-EM at 3.9 Å (55). It has been proposed that the relaxase has a dual role: in facilitating the DNA entry into the secretion channel and pulling it into the host cell.

The pilus is a dynamic structure formed by the polymerization of VirB2 (4). Recently the cryo-EM structures of two pili encoded by the F and F-like pED208 plasmids (at 5.0 Å and 3.6 Å, respectively) (28) revealed that they are formed by stacked layers of VirB2 pentamers (**Figure 4*d***). In these structures the additional density of phosphatidylglycerol (PG) was visible. This phospholipid is present in the pili in a 1:1 ratio with VirB2. Only the polar extremity of PG is exposed to the solvent; the rest of the molecule is buried in the proteinaceous structure. Its presence could facilitate dynamic processes such as the pilus fusion with the host membrane, its reinsertion in the donor cells, and eventually the pilus depolymerization.

Type IVB Secretion Systems: Lesson from *Legionella pneumophila*

As T4ASSs, T4BSSs are also used by human bacterial pathogens to secrete toxins. However, in T4BSS more subunits (up to 27) are necessary for an efficient substrate translocation. Their

archetype is the Dot/Icm system of *Legionella pneumophila* (60). *L. pneumophila*, which causes Legionnaires' pneumonia, disrupts phagosome physiology in order to survive and replicate in the phagosome (80).

Major differences separate the Dot/Icm locus from that of the *A. tumefaciens* T4SS. The few homologies include sequence similarity of the C-terminal regions of DotG and VirB10, and three similar ATPases. Recently, first insights on the Dot/Icm organization were obtained by in situ analysis of *L. pneumophila* cells by ECT and subtomogram averaging (45). The Dot/Icm formed concentric arcs in the periplasm (**Figure 4*e***). The external layer, the Hat, is in contact with the outer membrane, carrying flanking densities (α and β). A stem connects it with the internal layer, which presents lateral densities (γ). The stem inserts into a stalk that ends in the inner membrane. Other structures appear connected to the inner membrane: two lateral wings protruding into the periplasm and four vertical rods in the cytoplasm. The two curved layers were proposed to be the core complex of this T4BSS, composed of DotC, DotD, DotF, DotG, and DotH. The Hat was proposed to be equivalent to the O-layer of the core complex, made by the VirB10/DotG- homology region. The rods in the cytoplasm fit with the ATPase barrels of the $VirB_{3-10}$ structure. Despite these similarities, the sizes of the T4ASS and Dot/Icm structures are quite different and the α and β densities seem to be unique to the T4BSS, while γ partially matches the I-layer of the T4ASS core complex.

This pioneering ECT study revealed the first structural data for a T4BSS. The Dot/Icm system shows relevant similarities only with the T4ASS system, excluding any relation with other bacterial secretion systems. However, as suggested by its genetic complexity, this system differs greatly from the T4ASS. The structural basis of its secretion mechanism—key to understanding *L. pneumophila* pathogenicity—is expected to emerge as subunits are identified from structures with improved resolution.

The *Helicobacter pylori* cag Type IV Secretion System

Helicobacter pylori expresses four T4SSs: comB, tfs3, tfs4, and cag. The cag T4SS is encoded by pathogenicity islands (PAIs) in the bacterial genome. Its main substrate is the oncoprotein CagA, which alters the innate immune system, perturbing the homeostasis of gastric epithelial cells, causing ulcers, and increasing cancer risk. Genetic analyses suggest that the *H. pylori* PAI includes all the VirB/D4 orthologs and many more genes (7).

Like the VirB/D4 secretion machinery, the cag T4SS is composed of a CC including the *A. tumefaciens*–homologous CagX/VirB9 and CagY/VirB10 plus the subunits Cag3, CagT, and CagM. The cag CC has been purified and visualized by NS-EM showing the typical 14-fold symmetry but larger dimensions, comparable to the *L. pneumophila* Dot/Icm apparatus (39).

Recent ECT work investigated the cag T4SS in vivo. Images of intact *H. pylori* in coculture with human gastric epithelial cells showed tube-like appendages specific to the host-pathogen interaction (24). CC-like particles were observed on membrane regions near the tubes, presenting 14-fold symmetry and a diameter of 40 nm. The cag T4SS global organization presents a similar overall architecture as the Dot/Icm system, but with additional densities (δ) located below the Hat (**Figure 4*e***). The α and β densities form an upper ring and a lower ring, defining a more compact structure compared to the Dot/Icm. Four barrels surrounding a short central barrel in the cytoplasm were modelled. The lateral densities appear equivalent to the VirB4 ATPase, and the central barrel is suggested to be Cag5/VirD4.

These first structural characterizations of *H. pylori* cag T4SS suggest that this system is a hybrid of the T4ASS and the T4BSS (24, 39).

Chang et al. hypothesized that the complex they presented was assembled as a consequence of the host-pathogen interaction. In this model, the interaction with host cells would trigger a conformational change in the cag T4SS, detaching the Hat from the outer ring of the CC, while the pilus (composed of CagC) would grow surrounded by the outer membrane (24).

These promising advancements show how EM is revolutionizing the investigation of such challenging systems. However, many questions remain unanswered. More structural details are required to understand the different states of the machineries and the role of the pilus in secreting the effector into the host cell.

In conclusion, the last nine years reshaped our understanding of T4SSs, thanks mainly to the use of EM combined with the large body of data in the literature and X-ray crystallography. However, there are still several open questions about the localization of many subunits and the T4SS mechanism. More structures at higher resolution are necessary to understand how the substrates translocate through these modular systems.

THE TYPE VI SECRETION SYSTEM: A WEAPON OF BACTERIAL WARFARE

Bacteria that are capable of eliminating competitors are more effective at colonizing a niche. Those that express the T6SS benefit from being able to deliver effectors directly into competing bacteria (98). Moreover, toxin release occurs upon direct contact with any nonself cell, whether prokaryotic or eukaryotic, and results in its death. T6SSs differ from all other secretion systems because they can deliver several effectors to the target cell at the same time (104).

A T6SS can be seen as an inverted T4 bacteriophage contractile tail (**Figure 5*a***) (to which it is remotely homologous) (18). It consists of a membrane-tethering complex, a baseplate, a piercing needle or spike that carries the effectors to be secreted, a contractile sheath, and a rigid tube (see **Figure 5*b*,*c***).

The membrane-tethering complex is composed of three proteins: TssJ, TssL, and TssM. Two of these (TssL and TssM) share sequence homology with the type IV Dot/Icm proteins: IcmH/DotU and IcmF (34). The structure of the three components obtained by NS-EM consists of a large (20-nm) base that extends from the cytoplasm to the periplasm (**Figure 5*b*,*c***). It is attached to the outer membrane by a ring of 10 TssJ molecules and 10 elongated arches of TssM that extend to the inner base (**Figure 5*b*,*c***). The complex has a fivefold symmetry, and it is thought to open up to allow secretion to occur (33).

Once the tethering complex is assembled, it recruits proteins of the baseplate and the VgrG spike to the membrane (15). This complex, in turn, facilitates the nucleation of the proteins of the inner rigid tube (Hcp1) and the contractile sheath (TssB/TssC) capped by the dodecameric TssA protein (120) (**Figure 5*b*,*c***). The tube is composed of a contiguous assembly of Hcp1 hexamers that do not contain a twist in their structure (14). The sheath subunits TssB and TssC assemble onto the tube with an identical symmetry of six, but as helical polymers (14), in an extended, high-energy conformation (**Figure 5*d***). The sheath/tube assembly can reach a length of 1 μm, and it is thought that contact with the membrane at the opposite side of the cell provides the signal for the sheath polymerization to stop (9). Fluorescence experiments have shown that the assembly requires 20 s, whereas contraction of the sheath upon contact with a neighboring cell takes only 2 ms. Contraction of the sheath to a low-energy state leads to the release of the Hcp1 tube and piercing of the host membrane by the toxin-containing spike (9) (**Figure 5*a*,*d***).

An initial structure by single-particle cryo-EM of the contracted sheath from *V. cholerae* at 6 Å was obtained in 2014 (59). Later on, the resolution was improved to better than 4 Å in both *V. cholerae* and *Francisella tularensis*. the proteins were confirmed to be similar in structure to those of the T4 phage, and they assemble as a six-start helix, the handedness of assembly being the opposite of the phage tail (26, 62).

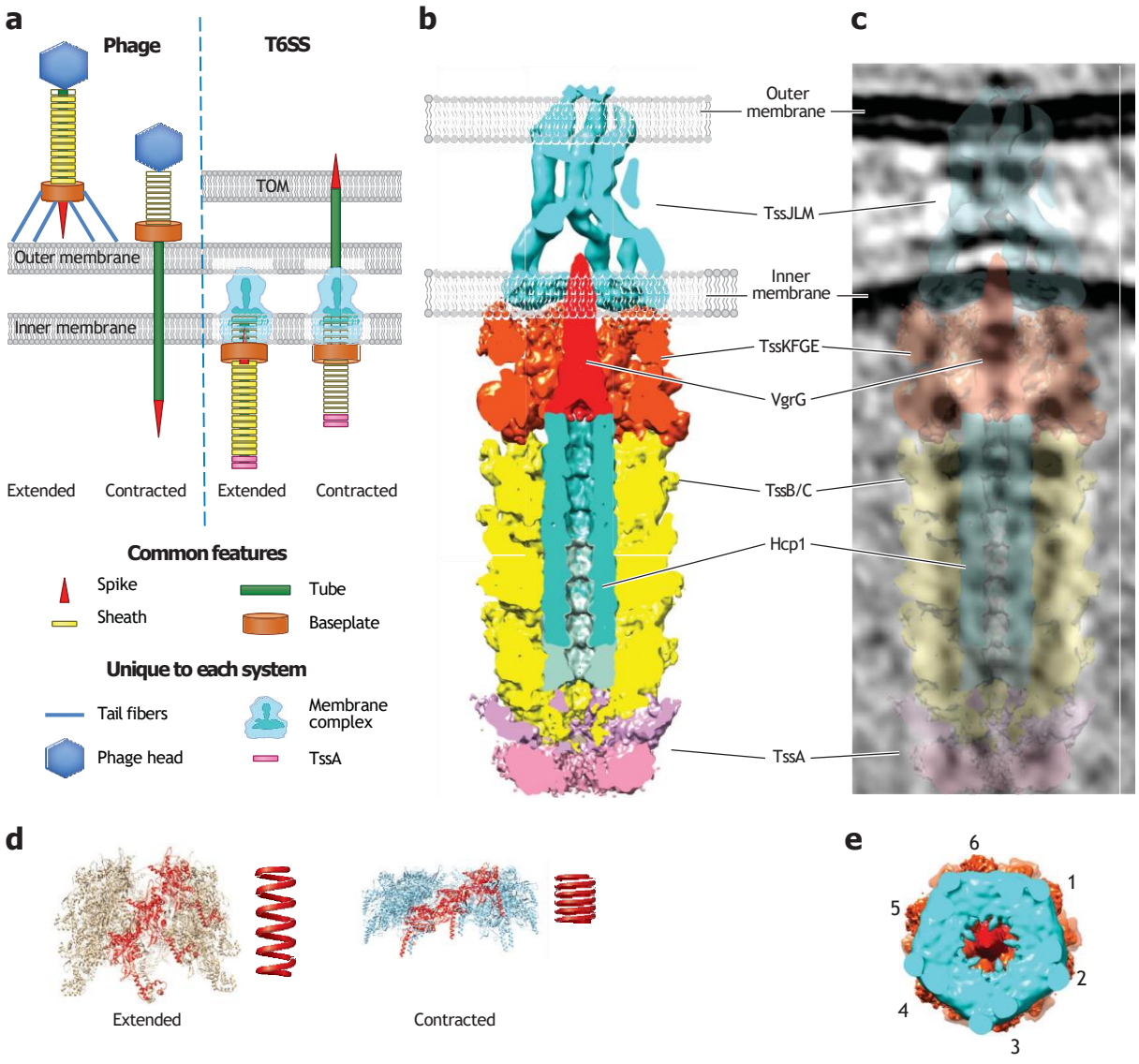

Figure 5

The type VI secretion system (T6SS), an inverted bacteriophage. (*a*) The T6SS has evolved from and can be considered as an inverted T4 phage. The regions that are conserved between the two apparatuses are the baseplate (*orange*), the sheath and the inner tube (*yellow*), and the spike (VgrG in *red*) that is required to pierce the membrane of the target cell (TOM). A unique component of the T6SS is the membrane complex that tethers the apparatus to the inner membrane (*cyan*). (*b*) Composite structures of the membrane complex, composed of TssJLM (*cyan*, Electron Microscopy Data Bank number EMD-2927), the baseplate (*orange*), made of TssKFGE, with the sheath (*yellow*) and inner tube (*green*), made of TssB/B and Hcp1, respectively (EMD-3879). The distal end of the sheath contains an extra density of a dodecameric structure that could be TssA (*pink*, EMD-3878). (*c*) Subtomogram averaging of the T6SS full complex in *Myxococcus xanthus* (EMD-8600); the structural elements are colored as in panel *b*. (*d*) Atomic structure of an extended (5MXN) and contracted (5MYU) sheath (*blue*) with one repeating unit in red, compared to a contracted and an extended spring coil. (*e*) Top view of the structure in panel *b*. The symmetry mismatch is evident between the pentameric TssJLM complex (*cyan*) and the hexameric baseplate, with numbers indicating the repeating subunits (*orange*).

A later cryo-EM SPA structure at 3.3 Å of distantly related sheath proteins from *P. aeruginosa* indicated that sequence differences do not affect the overall structure of the components and that the assembly is well conserved across species (99). Based on the available structures of the contracted and noncontractile sheath (112) (**Figure 5*d***), and based on homology to the T4 phage tail, it was possible to infer a mechanism of contraction that might resemble a coiled-spring motion (**Figure 5*d***). Such movement of the repeating units to an increased rotation and a decrease in rise produces −9.7 kcal/mol (99) and provides the energy to release the rigid tube out of the cell and into the neighboring cell. The structure of a noncontractile sheath with the Hcp1 tube in *V. cholerae* provided further evidence of the rotation of the sheath upon contraction (**Figure 5*d***), which exposes regions in the sheath protein that contain a recognition sequence for the disassembly and recycling of the monomers by ClpV (112).

While many structures of the most distinctive T6SS feature—the contractile sheath and tube—have been solved, the baseplate structure has proven more elusive. Recently the first structure of the sheath/tube/baseplate/distal end assembly to be obtained by single-particle cryo-EM, at an average of 7.5 Å, was published (79). It shows the baseplate on one end and a dodecameric ring at the distal end (**Figure 5*c***) that could be the multimeric TssA (88, 120). The limited resolution does not allow unambiguous assignment of individual components of the baseplate, but undoubtedly the structure will be used in the future for the placement of higher-resolution structures and will contribute to obtaining a full image of the complex.

Isolating the full complex for study by single-particle cryo-EM has been an impossible task because the sheath contracts and disassembles from the rest of the complex during cell disruption. While study of isolated components helps to infer the function and mechanism of action of each component, study of the full complex by ECT has also given a first glimpse of the fully assembled complex in *V. cholerae* (9) (**Figure 5*c***). It has allowed us to obtain a first model of the sheath in its contracted and extended states and to dock known structures into it to better understand the interaction between the different components in *Myxococcus xanthus* cells (22). Moreover, it was observed that the contractile injection system can exist even in the absence of a membrane-tethering complex, as in the case of *Amoebophilus asiaticus*. An integrative genetics and ECT study has allowed the identification in this species of a novel subtype of T6SSs derived from headless phages' extracellular contractile injection systems. This new system contains only a short inner membrane anchor module, the baseplate, and the sheath-tube assembly. This unusual system indicates that yet unrecognized T6SSs will need to be discovered (13).

The study of isolated components and the full complexes by SPA and ECT has advanced our understanding of the protein of effector secretion by the T6SS. Many questions remain, and a combination of techniques is required to answer them. High-resolution structures of the membrane complex and the baseplate are needed for mechanistic insight into the assembly and the contraction effect on the structures. Still to be determined is how a sixfold symmetry can be adapted to the fivefold symmetry of the membrane complex (**Figure 5*e***).

TYPE VII SECRETION SYSTEMS: THE SYSTEMS TO WATCH

The T7SSs were discovered in the vaccine strain *Mycobacterium bovis* BCG (bacillus Calmette-Gue´rin) (12). The region of difference missing in this attenuated strain (RD-1) includes *esx* genes encoding the ESX-1 T7SS machinery, which is directly involved in *Mycobacterium tuberculosis* virulence. The same locus includes genes encoding the secreted substrates ESAT-6/EsxA and CFP-10/EsxB (91), their associated Esp proteins, and members of the PE/PEE family (5, 115).

Genetic clusters related to the mycobacterial T7SS have been identified in other actinobacteria, in *Firmicutes*, and recently in gram-negative bacteria as well (109). In gram-positive *Firmicutes* these systems are called type VIIb secretion systems (T7bSSs). Despite a limited sequence homology, they share highly similar substrates, suggesting a common secretion mechanism. *M. tuberculosis* carries up to five paralogous T7SSs (ESX-1 to ESX-5) with distinct physiological functions. The better characterized among them are ESX-1 and ESX-5. ESX-1 takes part in the escape from the phagosome, and it is crucial for bacterial virulence. ESX-5 is present only in slow-growing mycobacteria, and it is involved in the host's immune response modulation and control of the bacterial capsule integrity (2, 6).

Six proteins are predicted to form the T7SSs: EccA, EccB, EccC, EccD, EccE, and MycP. All but the soluble ATPase EccA are membrane proteins. EccC is an ATPase belonging to the FtsK/SpoIIIE family. Its distal nucleotide-binding domain (NBD) binds the substrate EsxB, which regulates ATPase oligomerization and activity (97). MycP is a protease involved in maturation of the substrate EspB. The subunit EccD has 11 predicted transmembrane helices, and it is supposed to take part in the translocation channel. However, nothing is known about its precise role or the function of the other T7SS subunits, EccB and EccE.

The first insight into the general architecture of a T7SS came with the NS-EM model of a subcomplex of the *Mycobacterium xenopi* ESX-5 (11). $EccB_5$, $EccC_5$, $EccD_5$, and $EccE_5$ formed a complex of about 1.5 MDa organized as a hexamer around a pore of 5 nm, large enough to allow the translocation of folded EsxA/EsxB substrates (11) (**Figure 1*a***). EccB was docked in the core of the model using a previously obtained crystallographic structure of $EccB_1$ (119), protruding to the periplasm with a collar-like structure around the secretion channel. EccE was proposed to organize peripheral periplasmic densities. Immuno–gold labelling was used to identify the cytoplasmic part of the secretion machinery and to orient the complex with respect to the inner membrane. Although the integrity of the ATPase EccC was confirmed by mass spectrometry, its cytoplasmic domain, carrying three NBDs, was not solved in the structure, owing to high flexibility (11). The T7SS machinery is inserted into the inner membrane, leaving open the question about how substrates are secreted outside the cells. Interestingly, the ESX-1-specific substrate EspC is able to form filaments, and it might play a role in translocation of the substrates EsxA/EsxB through the mycobacterial outer membrane (71). The ESX-5 T7SS structure could be used as a model for further studies of other mycobacterial T7SSs. However, ESX-1 and T7bSSs present a quite different substrate repertoire; therefore, additional structural features might be associated to the secretion of specific effectors.

CONCLUSIONS AND OUTLOOK

Over the last ten years, advancements in EM combined with previously obtained biochemical data have propelled structural characterization of machineries that are required to secrete macro- molecules in bacteria and whose atomic mass is measured in mega-Daltons. Several notable struc- tures were solved at very high resolution, such as the T2SS secretin and T3SS basal body, which allowed for de novo model building of regions whose structure was previously unknown. For most secretion systems, a high-resolution structure by SPA cryo-EM is not yet available. This is due to biochemical instability of the complexes and low protein yields. SPA cryo-EM poses technical difficulties: It requires relatively large concentrations of proteins, and it relies on the stability of such complexes after isolation. Further technological developments in sample preparation, as well as deep biochemical characterization for these complexes, will undoubtedly increase the number of available structures. In some cases, to overcome purification issues and to visualize complexes in their native environment, structures of secretion complexes were solved by ECT. This technique

De novo model building: predicting the molecular composition of a protein from the electron density obtained by cryo-EM; usually only possible at <4 Å

in combination with SPA and crystallography allowed for known structures to be docked onto full complexes. At times, obtaining low-resolution envelopes of complexes (at nanometer resolution) by NS-EM is still the approach of choice, producing groundbreaking results, and it allows for placement of single components with reasonable accuracy (types IV, VI, and VII).

Because most secretion systems are associated with fitness, virulence, and antibiotics resistance in bacteria, targeting specific components of such machines with inhibitors or antimicrobial agents could hinder the pathogens without affecting the commensal population. For this purpose, further structural characterization of secretion systems through cryo-EM is crucial to increase the targets for development of an arsenal of new therapeutic compounds.

DISCLOSURE STATEMENT

The authors are not aware of any affiliations, memberships, funding, or financial holdings that might be perceived as affecting the objectivity of this review.

ACKNOWLEDGMENTS

We would like to thank Olivera Francetic and Julien Bergeron for critical discussion and comments on the manuscript, and Robin Anger for help with figures. We apologize to all the researchers whose work we did not include in the review because of space constraints. Work in the R.F. lab is supported by the CNRS, ERC, and IdeX. F.G. and M.T. are supported by the Unit of Microbiology directed by Pedro Alzari at the Institut Pasteur. F.G. is funded by the Institut Pasteur. C.R. is funded by IdeX, and M.T. is funded by the Pasteur Paris University (PPU) International PhD Program.

LITERATURE CITED

1. Abby SS, Cury J, Guglielmini J, Ne´ron B, Touchon M, Rocha EPC. 2016. Identification of protein secretion systems in bacterial genomes. *Sci. Rep.* 6:23080
2. Abdallah AM, Bestebroer J, Savage NDL, de Punder K, van Zon M, et al. 2011. Mycobacterial secretion systems ESX-1 and ESX-5 play distinct roles in host cell death and inflammasome activation. *J. Immunol.* 187(9):4744–53
3. Alvarez-Martinez CE, Christie PJ. 2009. Biological diversity of prokaryotic type IV secretion systems. *Microbiol. Mol. Biol. Rev.* 73(4):775–808
4. Arutyunov D, Frost LS. 2013. F conjugation: back to the beginning. *Plasmid* 70:18–32
5. Ates LS, Houben ENG, Bitter W. 2016. Type VII secretion: a highly versatile secretion system. In *Virulence Mechanisms of Bacterial Pathogens*, ed. IT Kudva, NA Cornick, PJ Plummer, Q Zhang, TL Nicholson, et al., pp. 357–84. Washington, DC: Am. Soc. Microb. 5th ed.
6. Ates LS, van der Woude AD, Bestebroer J, van Stempvoort G, Musters RJP, et al. 2016. The ESX-5 system of pathogenic mycobacteria is involved in capsule integrity and virulence through its substrate PPE10. *PLOS Pathog.* 12(6):e1005696
7. Backert S, Tegtmeyer N, Fischer W. 2015. Composition, structure and function of the *Helicobacter pylori cag* pathogenicity island encoded type IV secretion system. *Future Microbiol.* 10(6):955–65
8. Baron C, O'Callaghan D, Lanka E. 2002. Bacterial secrets of secretion: EuroConference on the biology of type IV secretion processes. *Mol. Microbiol.* 43:1359–65
9. Basler M, Pilhofer M, Henderson GP, Jensen GJ, Mekalanos JJ. 2012. Type VI secretion requires a dynamic contractile phage tail-like structure. *Nature* 483(7388):182–86
10. Bayliss R, Harris R, Coutte L, Monier A, Fronzes R, et al. 2007. NMR structure of a complex between the VirB9/VirB7 interaction domains of the pKM101 type IV secretion system. *PNAS* 104(5):1673–78
11. Beckham KS, Ciccarelli L, Bunduc CM, Mertens HD, Ummels R, et al. 2017. Structure of the mycobacterial ESX-5 type VII secretion system membrane complex by single-particle analysis. *Nat. Microbiol.* 2:17047. **https://doi.org/10.1038/nmicrobiol.2017.47**

12. Behr MA, Wilson MA, Gill WP, Salamon H, Schoolnik GK, et al. 1999. Comparative genomics of BCG vaccines by whole-genome DNA microarray. *Science* 284(5419):1520–23
13. Böck D, Medeiros JM, Tsao H, Penz T, Weiss GL, et al. 2017. In situ architecture, function, and evolution of a contractile injection system. *Science* 357(6352):713–17
14. Brunet YR, Henin J, Celia H, Cascales E. 2014. Type VI secretion and bacteriophage tail tubes share a common assembly pathway. *EMBO Rep*. 15(3):315–21
15. Brunet YR, Zoued A, Boyer F, Douzi B, Cascales E. 2015. The type VI secretion TssEFGK-VgrG phage-like baseplate is recruited to the TssJLM membrane complex via multiple contacts and serves as assembly platform for tail tube/sheath polymerization. *PLOS Genet*. 11(10):e1005545
16. Burghout P, Van Boxtel R Van Gelder P, Ringler P, Müller SA, et al. 2004. Structure and electrophysiological properties of the YscC secretin from the type III secretion system of *Yersinia enterocolitica*. *J. Bacteriol*. 186(14):4645–54
17. Cascales E, Atmakuri K, Sarkar MK, Christie PJ. 2013. DNA substrate-induced activation of the *Agrobacterium* VirB/VirD4 type IV secretion system. *J. Bacteriol*. 195(11):2691–704
18. Cascales E, Cambillau C. 2012. Structural biology of type VI secretion systems. *Philos. Trans. R. Soc. Lond. B. Biol. Sci*. 367(1592):1102–11
19. Cascales E, Christie PJ. 2004. Definition of a bacterial type IV secretion pathway for a DNA substrate. *Science* 304(5674):1170–73
20. Chami M, Guilvout I, Gregorini M, Re´migy HW, Müller SA, et al. 2005. Structural insights into the secretin PulD and its trypsin-resistant core. *J. Biol. Chem*. 280(45):37732–41
21. Chandran V, Fronzes R, Duquerroy S, Cronin N, Navaza J, Waksman G. 2009. Structure of the outer membrane complex of a type IV secretion system. *Nature* 462(7276):1011–15
22. Chang Y, Rettberg LA, Ortega DR, Jensen GJ. 2017. In vivo structures of an intact type VI secretion system revealed by electron cryotomography. *EMBO Rep*. 18(7):1090–99
23. Chang Y-W, Rettberg LA, Treuner-Lange A, Iwasa J, Søgaard-Andersen L, Jensen GJ. 2016. Architecture of the type IVa pilus machine. *Science* 351(6278):aad2001
24. Chang Y-W, Shaffer CL, Rettberg LA, Ghosal D, Jensen GJ. 2018. In vivo structures of the *Helicobacter pylori cag* type IV secretion system. *Cell Rep*. 23(3):673–81. **https://doi.org/10.1016/j.celrep.2018.03.085**
25. Christie PJ. 2016. The mosaic type IV secretion systems. *EcoSal Plus* 7(1):395–401
26. Clemens DL, Ge P, Lee B-Y, Horwitz MA, Zhou ZH. 2015. Atomic structure of T6SS reveals interlaced array essential to function. *Cell* 160(5):940–51
27. Collins RF, Davidsen L, Derrick JP, Ford RC, Tønjum T. 2001. Analysis of the PilQ secretin from *Neisseria meningitidis* by transmission electron microscopy reveals a dodecameric quaternary structure. *J. Bacteriol*. 183(13):3825–32
28. Costa TRD, Ilangovan A, Ukleja M, Redzej A, Santini JM, et al. 2016. Structure of the bacterial sex F pilus reveals an assembly of a stoichiometric protein-phospholipid complex. *Cell* 166(6):1436–44.e10
29. d'Enfert C, Ryter A, Pugsley AP. 1987. Cloning and expression in *Escherichia coli* of the *Klebsiella pneumoniae* genes for production, surface localization and secretion of the lipoprotein pullulanase. *EMBO J*. 6(11):3531–38
30. Douzi B, Filloux A, Voulhoux R. 2012. On the path to uncover the bacterial type II secretion system. *Philos. Trans. R. Soc. B Biol. Sci*. 367(1592):1059–72
31. Dubochet J, McDowall AW. 1981. Vitrification of pure water for electron microscopy. *J. Microsc*. 124(3):3–4
32. Dunstan RA, Heinz E, Wijeyewickrema LC, Pike RN, Purcell AW, et al. 2013. Assembly of the type II secretion system such as found in *Vibrio cholerae* depends on the novel Pilotin AspS. *PLOS Pathog*. 9(1):e1003117. **https://doi.org/10.1371/journal.ppat.1003117**
33. Durand E, Nguyen VS, Zoued A, Logger L, Pehau-Arnaudet G, et al. 2015. Biogenesis and structure of a type VI secretion membrane core complex. *Nature* 523(7562):555–60
34. Durand E, Zoued A, Spinelli S, Watson PJH, Aschtgen M-S, et al. 2012. Structural characterization and oligomerization of the TssL protein, a component shared by bacterial type VI and type IVb secretion systems. *J. Biol. Chem*. 287(17):14157–68

35. East A, Mechaly AE, Huysmans GHM, Bernarde C, Tello-Manigne D, et al. 2016. Structural basis of pullulanase membrane binding and secretion revealed by X-ray crystallography, molecular dynamics and biochemical analysis. *Structure* 24(1):92–104
36. Fan E, Chauhan N, Udatha DBRKG, Leo JC, Linke D. 2016. Type V secretion systems in bacteria. *Microbiol. Spectr.* 4(1):305–35
37. Fischer W, Haas R, Odenbreit S. 2002. Type IV secretion systems in pathogenic bacteria. *Int. J. Med. Microbiol.* 292(3–4):159–68
38. Frank J. 1975. Averaging of low exposure electron micrographs of non-periodic objects. *Ultramicroscopy* 1(2):159–62
39. Frick-Cheng AE, Pyburn TM, Voss BJ, McDonald WH, Ohi MD, Cover TL. 2016. Molecular and structural analysis of the *Helicobacter pylori* type IV secretion system core complex. *mBio* 7(1):e02001-15
40. Fronzes R. 2009. Structure of a type IV secretion system core complex. *Science* 323:266–68
41. Fronzes R, Christie PJ, Waksman G. 2009. The structural biology of type IV secretion systems. *Nat. Rev. Microbiol.* 7(10):703–14
42. Fronzes R, Schafer E, Wang L, Saibil HR, Orlova EV, Waksman G. 2009. Structure of a type IV secretion system core complex. *Science* 323(5911):266–68
43. Gala´n JE, Lara-Tejero M, Marlovits TC, Wagner S. 2014. Bacterial type III secretion systems: specialized nanomachines for protein delivery into target cells. *Annu. Rev. Microbiol.* 68:415–38
44. Gelvin SB. 2003. Agrobacterium-mediated plant transformation: the biology behind the "gene-jockeying" tool. *Microbiol. Mol. Biol. Rev.* 67(1):16–37
45. Ghosal D, Chang Y, Jeong KC, Vogel JP, Jensen GJ. 2017. In situ structure of the *Legionella* Dot/Icm type IV secretion system by electron cryotomography. *EMBO Rep*. 18(5):726–32
46. Goyal P, Krasteva PV, Van Gerven N, Gubellini F, Van den Broeck I, et al. 2014. Structural and mechanistic insights into the bacterial amyloid secretion channel CsgG. *Nature* 516(7530):250–53
47. Hay ID, Belousoff MJ, Dunstan RA, Bamert RS, Lithgow T. 2018. Structure and membrane topography of the *Vibrio*-type secretin complex from the type 2 secretion system of enteropathogenic *Escherichia coli*. *J. Bacteriol*. 200:e00521-17
48. Hay ID, Belousoff MJ, Lithgow T. 2017. Structural basis of type 2 secretion system engagement between the inner and outer bacterial membranes. *mBio* 8(5):e01344-17
49. Henderson R. 1995. The potential and limitations of neutrons, electrons and X-rays for atomic resolution microscopy of unstained biological molecules. *Q. Rev. Biophys.* 28(2):171–93
50. Henderson R, Baldwin JM, Ceska TA, Zemlin F, Beckmann E, Downing KH. 1990. Model for the structure of bacteriorhodopsin based on high-resolution electron cryo-microscopy. *J. Mol. Biol.* 213(4):899–929
51. Hobbs M, Mattick JS. 1993. Common components in the assembly of type 4 fimbriae, DNA transfer systems, filamentous phage and protein-secretion apparatus: a general system for the formation of surface-associated protein complexes. *Mol. Microbiol.* 10(2):233–43
52. Hu B, Lara-Tejero M, Kong Q, Gala´n JE, Liu J. 2017. In situ molecular architecture of the *Salmonella* type III secretion machine. *Cell* 168(6):1065–74.e10
53. Hu B, Morado DR, Margolin W, Rohde JR, Arizmendi O, et al. 2015. Visualization of the type III secretion sorting platform of *Shigella flexneri*. *PNAS* 112(4):1047–52
54. Hueck CJ. 1998. Type III protein secretion systems in bacterial pathogens of animals and plants. *Microbiol. Mol. Biol. Rev.* 62(2):379–433
55. Ilangovan A, Kay CWM, Roier S, El Mkami H, Salvadori E, et al. 2017. Cryo-EM structure of a relaxase reveals the molecular basis of DNA unwinding during bacterial conjugation. *Cell* 169(4):708–21.e12
56. Journet L, Agrain C, Broz P, Cornelis GR. 2003. The needle length of bacterial injectisomes is determined by a molecular ruler. *Science* 302:1757–60
57. Koo J, Burrows LL, Lynne Howell P. 2012. Decoding the roles of pilotins and accessory proteins in secretin escort services. *FEMS Microbiol. Lett.* 328:1–12
58. Koster M, Bitter W, de Cock H, Allaoui A, Cornelis GR, Tommassen J. 1997. The outer membrane component, YscC, of the Yop secretion machinery of *Yersinia enterocolitica* forms a ring-shaped multimeric complex. *Mol. Microbiol.* 26:789–97

59. Kube S, Kapitein N, Zimniak T, Herzog F, Mogk A, Wendler P. 2014. Structure of the VipA/B type VI secretion complex suggests a contraction-state-specific recycling mechanism. *Cell Rep.* 8(1):20–30
60. Kubori T, Koike M, Bui XT, Higaki S, Aizawa S-I, Nagai H. 2014. Native structure of a type IV secretion system core complex essential for *Legionella* pathogenesis. *PNAS* 111:11804–9
61. Kudryashev M, Stenta M, Schmelz S, Amstutz M, Wiesand U, et al. 2013. In situ structural analysis of the *Yersinia enterocolitica* injectisome. *eLife* 2:e00792. **https://doi.org/10.7554/eLife.00792**
62. Kudryashev M, Wang RY-R, Brackmann M, Scherer S, Maier T, et al. 2015. Structure of the type VI secretion system contractile sheath. *Cell* 160(5):952–62
63. Kuhlbrandt W. 2014. The Resolution Revolution. *Science* 343(6178):1443–44
64. Kuhlen L, Abrusci P, Johnson S, Gault J, Deme J, et al. 2018. Structure of the core of the type three secretion system export apparatus. bioRxiv 249128. **https://doi.org/10.1101/249128**
65. Lasica AM, Ksiazek M, Madej M, Potempa J. 2017. The type IX secretion system (T9SS): highlights and recent insights into its structure and function. *Front. Cell. Infect. Microbiol.* 7:215
66. Lawley TD, Klimke WA, Gubbins MJ, Frost LS. 2003. F factor conjugation is a true type IV secretion system. *FEMS Microbiol. Lett.* 224:1–15
67. Li X, Mooney P, Zheng S, Booth CR, Braunfeld MB, et al. 2013. Electron counting and beam-induced motion correction enable near-atomic-resolution single-particle cryo-EM. *Nat. Methods.* 10(6):584–90
68. Lindeberg M, Salmond G, Collmer A. 1996. Complementation of deletion mutations in a cloned functional cluster of *Erwinia chrysanthemi out* genes with *Erwinia carotovora out* homologues reveals OutC and OutD as candidate gatekeepers of species-specific secretion of proteins via the type II pathway. *Mol. Microbiol.* 20:175–90
69. Linderoth NA. 2008. Scanning transmission electron microscopy the filamentous phage pIV Multimer visualized by scanning transmission electron microscopy. *Science* 16351997:1635–38
70. Lo´pez-Castilla A, Thomassin J-L, Bardiaux B, Zheng W, Nivaskumar M, et al. 2017. Structure of the calcium-dependent type 2 secretion pseudopilus. *Nat. Microbiol.* 2(12):1686–95
71. Lou Y, Rybniker J, Sala C, Cole ST. 2017. EspC forms a filamentous structure in the cell envelope of *Mycobacterium tuberculosis* and impacts ESX-1 secretion. *Mol. Microbiol.* 103(1):26–38. **https://doi.org/10.1111/mmi.13575**
72. Low HH, Gubellini F, Rivera-Calzada A, Braun N, Connery S, et al. 2014. Structure of a type IV secretion system. *Nature* 508(7497):550–53
73. Majewski DD, Worrall LJ, Strynadka NC. 2018. Secretins revealed: structural insights into the giant gated outer membrane portals of bacteria. *Curr. Opin. Struct. Biol.* 51:61–72. **https://doi.org/10.1016/j.sbi.2018.02.008**
74. Makino F, Shen D, Kajimura N, Kawamoto A, Pissaridou P, et al. 2016. The architecture of the cytoplasmic region of type III secretion systems. *Sci. Rep.* 6:33341
75. Marlovits TC, Kubori T, Lara-Tejero M, Thomas D, Unger VM, Gala´n JE. 2006. Assembly of the inner rod determines needle length in the type III secretion injectisome. *Nature* 441(7093):637–40
76. Marlovits TC, Kubori T, Sukhan A, Thomas DR, Gala´n JE, Unger VM. 2004. Structural insights into the assembly of the type III secretion needle complex. *Science* 306(5698):1040–42
77. Morgan JLW, Acheson JF, Zimmer J. 2017. Structure of a type-1 secretion system ABC transporter. *Structure* 25(3):522–29
78. Nans A, Kudryashev M, Saibil HR, Hayward RD. 2015. Structure of a bacterial type III secretion system in contact with a host membrane in situ. *Nat. Commun.* 6:10114. **https://doi.org/10.1038/ncomms10114**
79. Nazarov S, Schneider JP, Brackmann M, Goldie KN, Stahlberg H, Basler M. 2017. Cryo-EM reconstruction of type VI secretion system baseplate and sheath distal end. *EMBO J.* 37:e97103
80. Ninio S, Roy CR. 2007. Effector proteins translocated by *Legionella pneumophila*: strength in numbers. *Trends Microbiol.* 15:372–80
81. Nivaskumar M, Bouvier G, Campos M, Nadeau N, Yu X, et al. 2014. Distinct docking and stabilization steps of the pseudopilus conformational transition path suggest rotational assembly of type IV pilus-like fibers. *Structure* 22(5):685–96
82. Nivaskumar M, Francetic O. 2014. Type II secretion system: a magic beanstalk or a protein escalator. *Biochem. Biophys. Acta* 1843:1568–77

83. Notti RQ, Stebbins CE. 2016. The structure and function of type III secretion systems. *Microbiol. Spectr.* 4(1):1–30
84. Nouwen N, Ranson N, Saibil H, Wolpensinger B, Engel A, et al. 1999. Secretin PulD: association with pilot PulS, structure, and ion-conducting channel formation. *PNAS* 96(14):8173–77
85. Nunn D. 1999. Bacterial type II protein export and pilus biogenesis: more than just homologies? *Trends Cell Biol*. 9(10):402–8
86. Park J, Zhang Y, Chen C, Dudley EG, Harvill ET. 2015. Diversity of secretion systems associated with virulence characteristics of the classical bordetellae. *Microbiology* 161(12):2328–40. **https://doi.org/10.1099/mic.0.000197**
87. Pineau C, Guschinskaya N, Robert X, Gouet P, Ballut L, Shevchik VE. 2014. Substrate recognition by the bacterial type II secretion system: more than a simple interaction. *Mol. Microbiol.* 94(1):126–40
88. Planamente S, Salih O, Manoli E, Albesa-Jove´ D, Freemont PS, Filloux A. 2016. TssA forms a gp6-like ring attached to the type VI secretion sheath. *EMBO J*. 35(15):1613–27
89. Pugsley AP. 1993. The complete general secretory pathway in gram-negative bacteria. *Microbiol. Rev.* 57(1):50–108
90. Pugsley AP, Kornacker MG, Poquet I. 1991. The general protein-export pathway is directly required for extracellular pullulanase secretion in *Escherichia coli* k12. *Mol. Microbiol.* 5(2):343–52
91. Pym AS, Brodin P, Brosch R, Huerre M, Cole ST. 2002. Loss of RD1 contributed to the attenuation of the live tuberculosis vaccines *Mycobacterium bovis* BCG and *Mycobacterium microti. Mol. Microbiol*. 46(3):709–17
92. Radics J, Ko¨nigsmaier L, Marlovits TC. 2014. Structure of a pathogenic type 3 secretion system in action. *Nat. Struct. Mol. Biol.* 21(1):82–87
93. Rapisarda C, Fronzes R. 2017. Secretion systems used by bacteria to subvert host functions. In *Bacterial Evasion of the Host Immune System*, ed. P Escoll, pp. 1–40. Poole, UK: Caister Acad.
94. Redzej A, Ukleja M, Connery S, Trokter M, Felisberto-Rodrigues C, et al. 2017. Structure of a VirD4 coupling protein bound to a VirB type IV secretion machinery. *EMBO J*. 36(20):e201796629
95. Reichow SL, Korotkov KV, Hol WGJ, Gonen T. 2010. Structure of the cholera toxin secretion channel in its closed state. *Nat. Struct. Mol. Biol.* 17(10):1226–32
96. Rivera-Calzada A, Fronzes R, Savva CG, Chandran V, Lian PW, et al. 2013. Structure of a bacterial type IV secretion core complex at subnanometre resolution. *EMBO J*. 32(8):1195–204
97. Rosenberg OS, Dovala D, Li X, Connolly L, Bendebury A, et al. 2015. Substrates control multimerization and activation of the multi-domain APTase motor of type VII secretion. *Cell* 161:501–12
98. Russell AB, Hood RD, Bui NK, LeRoux M, Vollmer W, Mougous JD. 2011. Type VI secretion delivers bacteriolytic effectors to target cells. *Nature* 475(7356):343–47
99. Salih O, He S, Planamente S, Stach L, MacDonald JT, et al. 2017. Atomic structure of type VI contractile sheath from *Pseudomonas aeruginosa. Structure* 26:329–336.e3
100. Sandkvist M, Bagdasarian M, Howard SP, DiRita VJ. 1995. Interaction between the autokinase EpsE and EpsL in the cytoplasmic membrane is required for extracellular secretion in *Vibrio cholerae. EMBO J*. 14(8):1664–73
101. Scheres SHW. 2012. RELION: implementation of a Bayesian approach to cryo-EM structure determination. *J. Struct. Biol.* 180(3):519–30
102. Schraidt O, Lefebre MD, Brunner MJ, Schmied WH, Schmidt A, et al. 2010. Topology and organization of the *Salmonella typhimurium* type III secretion needle complex components. *PLOS Pathog*. 6(4):e1000824
103. Schraidt O, Marlovits TC. 2011. Three-dimensional model of *Salmonella*'s needle complex at subnanometer resolution. *Science* 331(6021):1192–95
104. Shneider MM, Buth SA, Ho BT, Basler M, Mekalanos JJ, Leiman PG. 2013. PAAR-repeat proteins sharpen and diversify the type VI secretion system spike. *Nature* 500(7462):350–53
105. Spreter T, Yip CK, Sanowar S, Andre´ I, Kimbrough TG, et al. 2009. A conserved structural motif mediates formation of the periplasmic rings in the type III secretion system. *Nat. Struct. Mol. Biol.* 16(5):468–76
106. Tang G, Peng L, Baldwin PR, Mann DS, Jiang W, et al. 2007. EMAN2: an extensible image processing suite for electron microscopy. *J. Struct. Biol.* 157(1):38–46

107. Tosi T, Estrozi LF, Job V, Guilvout I, Pugsley AP, et al. 2014. Structural similarity of secretins from type II and type III secretion systems. *Structure* 22(9):1348–55
108. Trokter M, Waksman G. 2018. Translocation through the conjugative type 4 secretion system requires unfolding of its protein substrate. *J. Bacteriol.* 200:e00615-17
109. Unnikrishnan M, Constantinidou C, Palmer T, Pallen MJ. 2017. The enigmatic Esx proteins: looking beyond mycobacteria. *Trends Microbiol.* 25:192–204
110. Voulhoux R, Ball G, Ize B, Vasil ML, Lazdunski A, et al. 2001. Involvement of the twin-arginine translocation system in protein secretion via the type II pathway. *EMBO J.* 20(23):6735–41
111. Wan W, Briggs JAG. 2016. Cryo-electron tomography and subtomogram averaging. *Methods Enzymol.* 579:329–67
112. Wang J, Brackmann M, Castaño-Díez D, Kudryashev M, Goldie KN, et al. 2017. Cryo-EM structure of the extended type VI secretion system sheath-tube complex. *Nat. Microbiol.* 2(11):1507–12
113. Waters CM, Bassler BL. 2005. Quorum sensing: cell-to-cell communication in bacteria. *Annu. Rev. Cell Dev. Biol.* 21:319–46
114. Winstanley C, Hart CA. 2001. Type III secretion systems and pathogenicity islands. *J. Med. Microbiol.* 50(2):116–26
115. Wong K-W. 2018. The Role of ESX-1 in *Mycobacterium tuberculosis* pathogenesis. In *Tuberculosis and the Tubercle Bacillus*, ed. WR Jaccobs Jr., H McShane, V Mizrahi, IM Orme, pp. 627–34. Washington, DC: Am. Soc. Microbiol.
116. Worrall LJ, Hong C, Vuckovic M, Deng W, Bergeron JRC, et al. 2016. Near-atomic-resolution cryo-EM analysis of the *Salmonella* T3S injectisome basal body. *Nature* 540(7634):597–601
117. Yan Z, Yin M, Xu D, Zhu Y, Li X. 2017. Structural insights into the secretin translocation channel in the type II secretion system. *Nat. Struct. Mol. Biol.* 24(2):177–83
118. Yip C, Kimbrough T, Felise H, Vuckovic M, Thomas N, et al. 2005. Structural characterization of the molecular platform for type III secretion system assembly. *Nature* 435(7042):702–7
119. Zhang XL, Li DF, Fleming J, Wang LW, Zhou Y, et al. 2015. Core component EccB1 of the *Mycobacterium tuberculosis* type VII secretion system is a periplasmic ATPase. *FASEB J.* 29(12):4808–14
120. Zoued A, Durand E, Brunet YR, Spinelli S, Douzi B, et al. 2016. Priming and polymerization of a bacterial contractile tail structure. *Nature* 531(7592):59–63